Physica A 569 (2021) 125782

Contents lists available at ScienceDirect

Physica A

journal homepage: www.elsevier.com/locate/physa

Crack localization and the interplay between stress enhancement and thermal noise

Santanu Sinha [a,b], Subhadeep Roy [b], Alex Hansen [b,*]

[a] Beijing Computational Science Research Center, 10 East Xibeiwang Road, Haidian District, Beijing 100193, China
[b] PoreLab, Department of Physics, Norwegian University of Science and Technology, N-7491 Trondheim, Norway

ARTICLE INFO

Article history:
Available online 27 January 2021

Keywords:
Creep failure
Fiber bundle model
Percolation
Crack nucleation

ABSTRACT

We study the competition between thermal fluctuations and stress enhancement in the failure process of a disordered system by using a local load sharing fiber bundle model. The thermal noise is introduced by defining a failure probability that constitutes the temperature and elastic energy of the fibers. We observe that at a finite temperature and low disorder strength, the failure process, which nucleates in the absence of any thermal fluctuation, becomes spatially uncorrelated when the applied stress is sufficiently low. The dynamics of the model in this limit lies closely to the universality class of ordinary percolation. When applied stress is increased beyond a threshold value, localized fractures appear in the system which grow with time. We identify the boundary between the localized and random failure process in the space of temperature and applied stress, and find that the threshold of stress corresponding to the onset of localized crack growth increases with the increase of temperature.

One of us (AH) did a postdoc in Professor Dietrich Stauffer's group in 1987–1988. Before arriving from a postdoc at the ENS in Paris, he sent me a photo from Canada (via snail mail) where he was visiting with the following note on the back: "Dietrich Stauffer, trying to find Boulevard Saint Michel on the frozen seashore near St. Francis Xavier University, Nova Scotia, Canada. At least it is good training for future visits in Norway. D. S". For me, this sums up the Stauffer that we all knew and appreciated so much.

1. Introduction

Growth of fractures under external stress in heterogeneous materials, such as concrete or fiber-reinforced composites, depends on the interplay between material disorder and local stress concentration throughout the failure process. The heterogeneities compete with the local stress enhancement preventing the growth of a single unstable crack until the stress exceeds a critical value, beyond which it undergoes a catastrophic failure [1]. In addition to material heterogeneities, external time-dependent disturbances such as thermal fluctuations can also induce disorder in the system. These combined with an applied stress or strain can cause failure over time even if the applied stress is below the critical value [2]. This phenomenon is known as creep failure. The study of creep failure is an essential but notoriously difficult subject that has important engineering applications. Of special importance is the statistics connected to the time elapsed until creep failure occurs, the creep lifetime [3,4].

The underlying physical mechanisms behind the creep are the accumulation of plastic strain and damage in the system over time. In order to model the creep failure in disordered systems, mechanisms for such aging processes are needed

* Corresponding author.
E-mail addresses: santanu.sinha@ntnu.no (S. Sinha), subhadeep.roy@ntnu.no (S. Roy), alex.hansen@ntnu.no (A. Hansen).

https://doi.org/10.1016/j.physa.2021.125782

to be taken into account in addition to the structural heterogeneities. However, fracture in heterogeneous solids is yet difficult to handle with elasticity theory and therefore alternative approaches have been proposed. The Voight model [5] for precursory strain has been explored by Main [6] in order to understand the sub-critical crack growth dynamics. The model can reproduce the time-dependent strain rate observed in experiments [7]. A rather simple and intuitive model for disordered solids that has high numerical efficiency and analytical tractability is the fiber bundle model [8–14]. In this model, a set of fibers carry an external load which, upon the break of a fiber, is distributed to the surviving fibers globally (equal load sharing, ELS) or locally (local load sharing, LLS). Introducing thermal fluctuations by probabilistic noise, thermally activated failures have been investigated widely with this model for the global load sharing case [15–20]. These studies have explained the time-dependent strain rate and showed how the temperature plays a crucial role in the creep lifetime. Danku and Kun considered a damage accumulation process in each fiber by introducing a damage variable and a time evolution equation in ELS [21]. Thermally driven failure for the localized load sharing process was studied by Yoshioka et al. [22,23] with Gaussian distributed thermal fluctuations where they showed that, unlike the ELS, the failure time in LLS exhibits anomalous scaling with the system size. Phase boundaries between different regimes of failures were also explored depending on the temperature and applied load. However, those studies were performed for homogeneous systems in the absence of any quenched disorder in the fiber strengths. Hidalgo et al. [24,25] studied creep in a viscoelastic fiber bundle model by introducing a time evolution equation for the strain that is based on the Kelvin–Voigt rheology and highlighted the different behaviors in ELS and LLS. Recently, Roy and Hatano have showed that the fiber bundle model can also exhibit creep-like behavior in the absence of any thermal fluctuations, damage variables or rheological constitutive laws where time-dependent strain rate can be obtained [26,27].

In this work, we explore the creep failure due to thermal fluctuations in a fiber bundle model with localized load distributions. The bundle here contains quenched disorder in the failure thresholds whereas the thermal noise introduces time-dependent annealed disorder. We introduce the thermal noise in the model by a probabilistic algorithm that is based on the elastic energy and the breaking energy of a fiber. These two disorders compete with the inhomogeneous stress distributions that is caused by the local load sharing process and create non-trivial failure dynamics. More specifically, we show that the introduction of thermal noise makes the failure process non-localized at the low system disorder, which otherwise would be localized in the absence of thermal fluctuations. We characterize the non-localized growth regime by measuring the geometrical properties of the cracks and show that they belong to the percolation universality class. The failure becomes localized at high external stress. We identify the boundary between the localized and non-localized regimes in the temperature vs applied stress plane. In the following, we present the model in Section 2 and the numerical results in Section 3 where we also discuss the results. We conclude in Section 4.

2. Model description

The fiber bundle model consists of N Hookean springs or *fibers* placed in between two clamps under an external force F carried by the fibers. The extension x_i of a fiber i under a force f_i follows the relation $f_i = \kappa x_i$. All the fibers have the same elastic constant κ but different maximum extension ϵ_i. If this value is exceeded, that particular fiber fails. The distribution of the thresholds ϵ_i among the fibers models the heterogeneity of the material. When a fiber fails, the load it was carrying is distributed among the surviving fibers according to a load-sharing scheme that models the way the forces are distributed among the surviving fibers. If the load carried by the failed fibers is distributed uniformly over all the surviving fibers, we have the *Equal Load Sharing* (ELS) scheme. With this scheme, there is no local stress enhancement in the model. On the other hand, if the load carried by the failed fiber is distributed evenly among the fibers bordering the cluster of broken fibers to which the failed fiber belong, we are dealing with the *Local Load Sharing* (LLS) scheme. Here local stress enhancement competes with the local heterogeneity. The ELS fiber bundle model was initially introduced by Peirce [8] to model the strength of yarn and since Daniels' paper [9], the model caught on in the mechanics community. Sornette introduced the ELS fiber bundle model to the statistical physics community in 1992 [28] which lead the community to explore the rich avalanche statistics [29–32] and analytical tractability of the ELS model. The local load-sharing (LLS) fiber bundle model was introduced by Harlow and Phoenix [33,34] as a one-dimensional array of fibers. There are also intermediate models between ELS and LLS models, e.g. the model by Hidalgo et al. [35], where the load of the failing fiber is distributed according to a power law in the distance from the failed fiber. Another is the soft clamp model [36–39], where the infinitely stiff clamps are replaced by clamps with finite elastic constant causing the load of the failing fiber to be distributed among the surviving in accordance with the elastic response of the soft clamps.

Here we consider an LLS fiber bundle model that is based on a history independent redistribution scheme [40] so that the complete stress field at any instance can be calculated from the present arrangement of intact and broken fibers without knowing any information about the order in which the fibers failed. For this, we define a *crack,* which is a cluster of s failed fibers defined as in percolation theory [41,42]. The *perimeter* of the crack is the set of h intact fibers that are nearest neighbors to the failed fibers in that crack. These nearest neighbors define the *hull* of the cluster [43]. The force on an intact fiber i at any instance is then calculated by

$$f_i = f\left(1 + \sum_{J(i)} \frac{s_{J(i)}}{h_{J(i)}}\right), \tag{1}$$

where $f = F/N$, the force per fiber. The summation runs over all the cracks $J(i)$ that are neighbors to the fiber i.

We will study the fiber bundle at a temperature T subjected to a constant external stress F that is less than the critical breaking stress for the bundle. For this, we introduce thermal fluctuation in the failure criteria of the LLS model. Due to thermal noise, a fiber i may fail even if the force on it fulfills $f_i < \kappa\epsilon_i$. The elastic energy of a fiber at extension x_i is $\kappa x_i^2/2$ and the elastic energy at failure is $\kappa\epsilon_i^2/2$. This energy is dissipated, i.e., lost as elastic energy at failure. We introduce a discrete time variable t to be defined below. We define a failure probability

$$P_i(t,T) = \exp\left[-\frac{\kappa(\epsilon_i^2 - f_i^2)}{2k_BT}\right], \tag{2}$$

where k_B is the Boltzmann constant. In the following we set $\kappa/k_B = 1$ for simplicity. The simulation starts at $t = 0$ with all fibers intact and each carrying a finite load $f_i = f$. The failure probability P_i is then calculated for each fiber i. We then generate a random number r_i uniformly distributed between 0 and 1 for each fiber i, which we compare to P_i. All the fibers for which $r_i < P_i$ fails at that time step. The forces are then redistributed according to Eq. (1) and time t is increased by 1. With this dynamics, multiple fibers can therefore break at the same time step. This procedure is repeated until all fibers have failed. Note that the failure probability P_i is an increasing function of the temperature T as well as of the local stress f_i which also increases with time due to the failures. The number of fibers that break at the same time step therefore increases with the increase in temperature. When $f_i > \epsilon_i$, P_i is always greater than one for any temperature T and the fiber always breaks. Furthermore, as the temperature is changed towards zero ($T \to 0$), the failure probability P_i is approached towards a step function from 0 to 1 at $f_i = \epsilon_i$. This means, at $T = 0$, there is no contribution from the thermal noise to the breaking probability and a fiber only breaks due to the local stress. This leads the model to approach the conventional LLS model at $T = 0$ [44]. With increasing temperature, P_i increases throughout the range of f_i and becomes less dependent on how f_i is close to the threshold ϵ_i. Recently, a similar probabilistic failure process was adopted to explore the creep failure in ELS fiber bundle model [45].

For the disorder in the failure thresholds ϵ_i, we consider a distribution that has only one control parameter. The thresholds in this distribution are generated by calling a random number (r_i) over the unit interval and raising it to a power D, therefore $\epsilon_i = r_i^D$. This corresponds to the cumulative distribution [46,47],

$$P(\epsilon) = \begin{cases} \epsilon^{1/|D|}\,, \epsilon \in [0,1] & \text{when } D > 0\,, \\ 1 - \epsilon^{-1/|D|}\,, \epsilon \in [1,\infty) & \text{when } D < 0\,. \end{cases} \tag{3}$$

The strength of disorder in this distribution is controlled by the value of $|D|$. Moreover, $D > 0$ and $D < 0$ respectively correspond to the distributions with power law tails towards weaker and stronger fibers and $D = 1$ returns a uniform distribution. With this distribution, the interplay between system disorder and local stress enhancement in LLS fiber bundle model in the absence of any thermal noise was explored recently [44]. There, phase transitions from a localized fracture regime to random fractures were observed while increasing the disorder. Interestingly, the transition for $D < 0$ was of first order and for $D > 0$ was of second order. In the present work, we investigate the effect of thermal noise on the failure dynamics and study its effect on crack localization, and we limit our simulations in the low disorder limit at $D = 0.02$, where the failure was localized in the absence of temperature. As we will see in the next section, that the presence of temperature makes the fracture growth non-localized in this regime when the stress is low. We present our numerical results in the following.

3. Results

We consider a bundle of $N = 256 \times 256$ fibers in two dimensions (2D) with periodic boundary conditions. The results are averaged over 1000 realizations of samples. Simulations are performed for different values of temperature (T) and external stress ($f = F/N$) which are kept constant throughout a simulation. The thermal noise initiates a creep failure process to break the system over time even if the applied stress is less than the critical value. Depending on the thermal noise and local stress enhancements, many or few fibers may fail simultaneously. The growth of damage in this process is illustrated in Fig. 1 where we plot the damage d — defined as the number of failed fibers divided by N — as a function of t for a stress $f = 0.08$, which is lower than the critical stress in the absence of thermal fluctuations. The plot shows three stages of failure process, a primary stage where the rate of damage decreases with time, a secondary stage where the damage rate is almost constant, and a tertiary stage where the damage increases rapidly until the whole bundle fails. This is a qualitative characteristics that is generally observed during a creep failure [13]. The red dot at the end of the curve indicates the failure time t_f which depends on the temperature as well as on the applied stress. This is shown in the inset, where t_f decreases with increase of both T and f, as a higher stress or temperature generates higher probability of failure at each time step, making the model to approach the global failure faster. When varying the temperature, the damage curve shows the similar shape within the range of temperature considered here. This is shown in Fig. 1(b) for $f = 0.10$ where all the three stages of creep can be observed. However, the shape of plot changes drastically when the applied stress is increased, which is shown in Fig. 1(c). We will see in the following that the increase in the applied stress initiates a localized failure regime. We see in this regime that the damage increases almost constantly with time since the beginning of the failure process indicating the absence of the primary creep. The deformation rate during the secondary

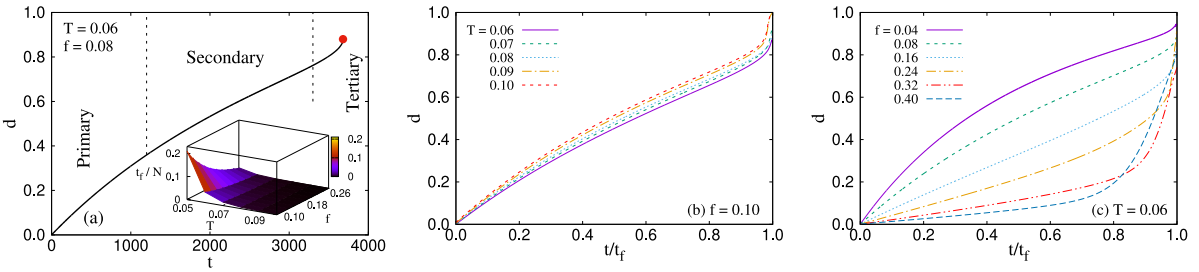

Fig. 1. The variation of damage d with time t is shown in (a) for $T = 0.06$ and $f = 0.08$ corresponding to the non-localized failure regime. The plot shows three regimes of creep like failure, the primary, secondary and tertiary regimes. The red dot shows the final failure point. The x-coordinate of this point corresponds to the failure time t_f. The inset of the figure shows how t_f decreases with the increase of temperature and applied stress. In (b), we show how the plot changes with the temperature in this non-localized regime. When increasing the applied stress, localized failures starts to appear, which changes the shape of the curve as shown in (c).

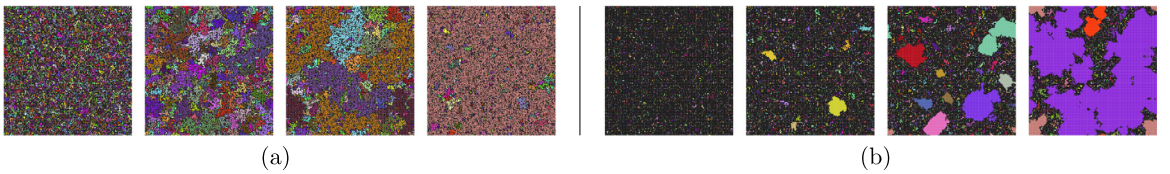

Fig. 2. Growth of cracks for two different applied stresses (a) $f = 0.1$ and (b) $f = 0.4$ in a bundle of 256×256 fibers at temperature $T = 0.06$. The thresholds are generated according to Eq. (3) at low disorder $D = 0.02$. The snapshots correspond to $t = 0.40t_f$, $0.60t_f$, $0.64t_f$ and $0.68t_f$ for $f = 0.1$, and $t = 0.48t_f$, $0.70t_f$, $0.79t_f$ and $0.87t_f$ for $f = 0.4$. The intact fibers are colored by black and the other colors represent different clusters of broken fibers. At low applied stress, cracks appear randomly in the system whereas at high applied stress localized cracks are observed to grow within the system.

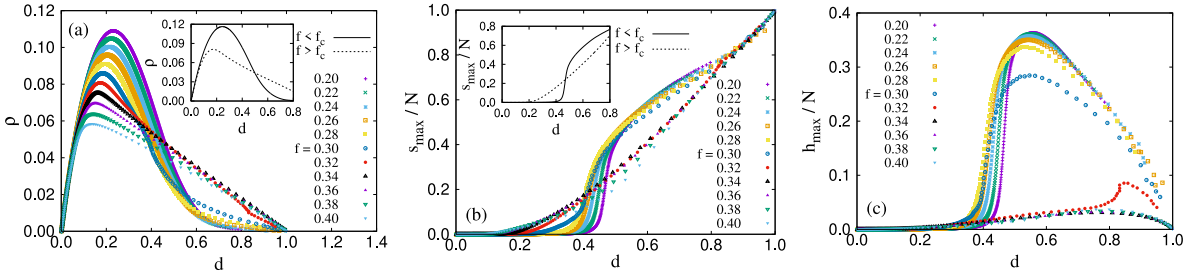

Fig. 3. (a) Variation of cluster density ρ with damage d for $T = 0.06$ while varying the applied stress f. Two distinct behaviors are observed for the non-localized and localized regimes corresponding to $f < f_c$ and $f > f_c$ respectively where $f_c = 0.30$. These two behaviors are highlighted in the inset for $f = 0.20$ and 0.32. (b) Variation of the maximum crack size s_{max} normalized by the system size N, with damage d. The inset highlights the two different behaviors below and above f_c. (c) Variation of the normalized maximum hull size h_{max}/N with damage d. Notice that, the maxima of h_{max} for non-localized regime have much higher values compared to the localized regime indicating a fractal structure of the clusters at $f < f_c$.

creep is directly related to the failure time t_f [13]. In the absence of system disorder, t_f scales as a power law of the system size for local load sharing where the power-law exponent is a function of the temperature and the applied stress [22]. The presence of the system disorder here can have a different effect on the power law and may be reported in a different study.

3.1. Localized vs non-localized fracture growth

The growth of cracks with time in the presence of temperature at two different external stress $f = 0.1$ and $f = 0.4$ are shown in Fig. 2. The intact clusters are colored by black and the individual clusters of failed fibers are marked with different colors. The pictures show two distinct regimes of crack growth. At low applied stress the subsequent failure events appear randomly in space, similar to the growth of percolation clusters. The clusters merge with time and a spanning cluster appears in the system similar to a percolating cluster that contains clusters of intact fibers of different sizes inside it. On the other hand, at high stress, localized clusters of failed fibers appear and they eventually merge together. The localized clusters in this case are compact.

To study how the applied stress and temperature alter the failure dynamics from random fractures to localized crack growth, we measure three different geometrical quantities, the number density of clusters, the largest cluster size and the

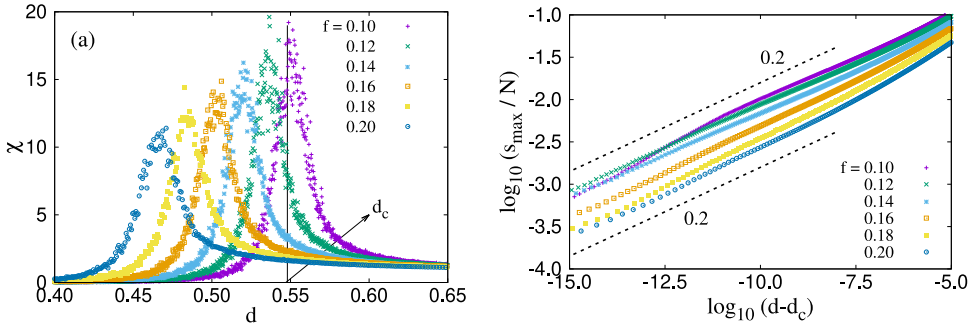

Fig. 4. (a) The response function χ, i.e., the rate of change of largest cluster size $s_{\max}$ as a function of the damage d. This is obtained by taking the derivative of $s_{\max}$ with respect to d with central difference technique. From the position of the peaks, we find the values of critical damage d_c. In (b), we plot $s_{\max}/N$ with $(d - d_c)$ where the slopes correspond to the exponent β defined in Eq. (4). We observe β around 0.2, which however fluctuates with the applied stress. The full list of the values of β for different applied stress will be given in Table 1.

largest perimeter size as a function of damage d for different values of T and f. They are plotted in Fig. 3(a), (b) and (c) respectively. In 3 (a), we plot the cluster number density ρ as a function of d for different applied stress (f) at temperature $T = 0.06$. Here ρ is defined as the number of clusters of failed fibers divided by the total number of fibers N, which shows a non-monotonic behavior with d. We observe $\rho = 0$ at $d = 0$ and $\rho = 1$ as $d \to 1$, because all the fibers are then broken creating a single crack. In between, ρ reaches a maximum value where the system contains maximum number of clusters. This maximum decreases with increase in f, and interestingly, the dependence of ρ on d shows a characteristic difference beyond an applied stress $f > f_c$ indicating a difference in the failure dynamics. These two different characteristics are highlighted in the inset for $f = 0.20$ and 0.32.

Next we measure the largest cluster size ($s_{\max}$) and the largest perimeter size ($h_{\max}$) as a function of d. In Fig. 3(b) and (c), we plot $s_{\max}$ and $h_{\max}$ respectively, scaled by the number of fibers N. As we vary the applied stress f, both the quantities show a characteristic difference in the behavior below and above f_c. In the beginning of the process, small fractures appear in the system leading to small values of $s_{\max}$, which will eventually grow and merge with each other. For $f > f_c$, the increase in $s_{\max}$ starts at a much earlier point than that of $f < f_c$. This reflects the appearance of compact localized cracks early in the system for $f > f_c$, which grow more uniformly with time. Whereas for $f < f_c$, spatially uncorrelated failures occur at random in space preventing the appearance of a large cluster for a longer duration. At some point of time, these small clusters start to coalesce causing a sharp increase in $s_{\max}$ as seen in the figure. When the coalescence is over after creating a large crack in the system, $s_{\max}$ grows in a linear manner. Behavior of $s_{\max}$ shows similarity with that of percolation model for $f < f_c$ whereas above f_c it deviates from such characteristic shape indicating the initiation of localization. These two behaviors for $f < f_c$ and $f > f_c$ are highlighted in the inset. The behavior of $h_{\max}$ shows a more interesting picture. It shows two different behavior for $f < f_c$ and $f > f_c$, however, the values of $h_{\max}$ are much smaller for $f > f_c$, that is in the localized regime. This indicates fractal type perimeter structure for $f < f_c$ compared to the perimeters of the localized cracks for $f > f_c$. Later in Section 3.3, we will use $h_{\max}$ to calculate the values of f_c and will show how the boundary between the non-localized and localized fracture regimes vary with the temperature T. For $f < f_c$, both $s_{\max}$ and $h_{\max}$ indicate percolation type dynamics during the failure process which we will explore in detail in the following.

3.2. Characterization of non-localized cluster growth for $f < f_c$

To characterize the growth of fractures in the non-localized regime we will now study the clusters geometries by using the percolation framework [41,42]. We performed simulations at $T = 0.06$ at different values of $f < f_c$. We found $f_c \approx 0.3$ for $T = 0.06$ and therefore considered $f = 0.10$, 0.12, 0.14, 0.16 and 0.18 for these simulations. To find a percolation threshold or a critical damage d_c, one can calculate the order parameter P_∞ defined as the probability that a site belongs to an infinite cluster. P_∞ can be measured from the number of sites ($s_{\max}$) that belong to the largest cluster and then by estimating $P_\infty = \lim_{N\to\infty} P_N$ where $P_N = s_{\max}/N$ averaged over all configurations. Ideally, P_∞ approaches to 0 from 1 continuously as $d \to d_c$ from above. In our case, we have a finite system of 256^2 fibers and therefore $P_N = s_{\max}/N$ does not meet to 0 sharply at a particular value of d (Fig. 3(b)). We therefore measure the percolation threshold d_c from the maximum of the response function χ of P_N, that is when the rate of change of $s_{\max}$ with d is maximum. This is plotted in Fig. 4(a) where the peaks of the plots determine the values of d_c for different f. As $d \to d_c$ from above, P_∞ approaches to zero with a critical exponent β defined as,

$$P_\infty \sim (d - d_c)^\beta \ . \tag{4}$$

In Fig. 4, we plot $s_{\max}/N$ as a function of $(d - d_c)$ for different values of f and from the slopes we find β in the range of 0.18 to 0.23 with error bars ranging between 0.04 to 0.07 (see Table 1). For site percolation, $\beta = 5/36$.

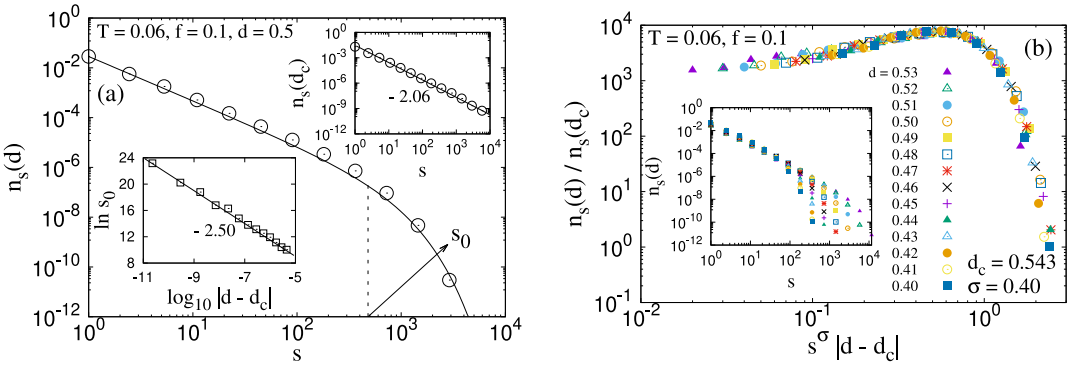

Fig. 5. (a) Plot of cluster size distribution $n_s(d)$ at $d = 0.5$ for $T = 0.06$ and $f = 0.10$. The circles represent simulation data and the solid line represents least square fitting of the data with Eq. (8), where τ is 2.06. The value of τ is obtained from the distribution $n_s(d_c)$ using Eq. (6) as shown in the upper inset of (a). We obtain the values of s_0 from the least-square fitting for different values of d. The variation of s_0 with $|d - d_c|$ is shown the inset, the slope of which corresponds to $1/\sigma$ (Eq. (9)). In (b), we plot the scaled cluster size distribution $n_s(d)/n_s(d_c)$ as a function of the scaled variable $s^\sigma |d - d_c|$ for $T = 0.06$ and $f = 0.10$ where we have used $\sigma = 1/2.50 = 0.40$ obtained from the previous plot. Here d_c is 0.543. In the inset, we show the unscaled behavior of $n_s(d)$ vs s for different values of d.

Next, we study the distribution of clusters of failed fibers near the critical damage d_c and investigate the scaling behavior of its moments. The cluster size distribution function $n_s(d)$ is defined as the number of s-sized finite clusters per lattice site at a damage $d \leq d_c$. According to scaling hypothesis [41,42], the functional form of the distribution can be assumed as,

$$\frac{n_s(d)}{n_s(d_c)} \sim \Phi\left[s^\sigma |d - d_c|\right] \ , \tag{5}$$

where $n_s(d_c)$ is the cluster size distribution at the critical damage d_c and σ is a critical exponent. This $n_s(d_c)$ at the critical damage shows a power-law decay,

$$n_s(d_c) \sim s^{-\tau} \ , \tag{6}$$

where τ is the cluster size distribution exponent. Using this in Eq. (5), we have the functional form for $n_s(d_c)$,

$$n_s(d) \sim s^{-\tau} \Phi\left[s^\sigma |d - d_c|\right] \tag{7}$$

as $d \to d_c$. Away from the critical damage, $n_s(d_c)$ falls with an exponential cut off with the following form,

$$n_s(d) \sim s^{-\tau} \exp\left(-\frac{s}{s_0}\right) \ , \tag{8}$$

where s_0 is the exponential cut off. As $d \to d_c$, s_0 generally shows the power law dependency,

$$s_0 \sim |d - d_c|^{-1/\sigma} \ . \tag{9}$$

To verify the scaling functional form for the cluster size distribution, we first measure the distribution of clusters at the critical point d_c. We then estimate the exponent τ by using Eq. (6) as shown in the upper inset of Fig. 5(a). Using this value of τ, we plot in Fig. 5(a) $n_s(d)$ as a function of s for $d = 0.5$. There we used least square fitting of the data points with the functional form given in Eq. (8) and estimated s_0 for different values of d. We then plot s_0 as a function of $|d - d_c|$ as shown in the lower inset of Fig. 5(a) and determine the exponent $\sigma = 0.40$ from the slope (Eq. (9)). With this value of σ, we verify the scaling function form given in Eq. (5). In Fig. 5 (b), we plot the scaled cluster size distribution $n_s(d)/n_s(d_c)$ as a function of the scaled variable $s^\sigma |d - d_c|$ for $T = 0.06$ and $f = 0.10$ where σ is taken as 0.40. We observe a data collapse for different values of $|d - d_c|$ and s showing the validity of Eq. (5). In the inset, we plot the unscaled values of $n_s(d)$ which show the approach of the power law behavior given in Eq. (7) as $d \to d_c$.

The kth *moment* of the cluster-size distribution, $M_k = \sum_s' s^k n_s(d)$ shows the singularity,

$$M_k \sim |d - d_c|^{(\tau - 1 - k)/\sigma} \tag{10}$$

as $d \to d_c$. The primed summation for M_k indicates the summation over finite clusters. The first moment, $k = 1$ represents the percolation probability P_∞. We measure the next three moments for $k = 2$, 3 and 4, where $k = 2$ corresponds to the average cluster size [48,49]. As $d \to d_c$, the moments M_2, M_3 and M_4 diverge with their respective critical exponents γ, δ and η defined as,

$$M_2 \sim |d - d_c|^{-\gamma} \quad , \qquad M_3 \sim |d - d_c|^{-\delta} \qquad \text{and} \qquad M_4 \sim |d - d_c|^{-\eta} \ . \tag{11}$$

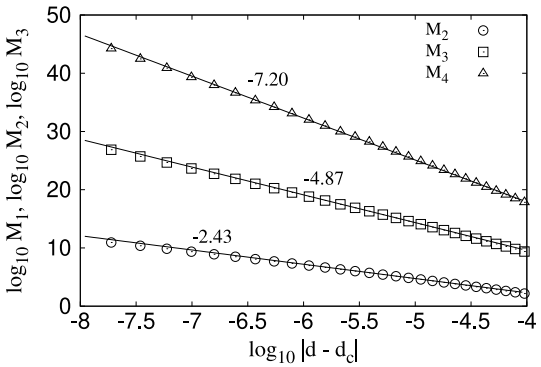

Fig. 6. Plot of the second, third and fourth moments M_2, M_3 and M_4 of cluster size distribution function as a function of $|d - d_c|$ for $T = 0.06$ and $f = 0.10$. From the slopes, we obtain the exponents, $\gamma = 2.43 \pm 0.03$, $\delta = 4.87 \pm 0.05$ and $\eta = 7.20 \pm 0.07$.

Table 1
List of the threshold damage and critical exponents obtained for different applied stress in the non-localized regime. Exponents are close to those observed in 2D percolation model where $\beta = 5/36$, $\gamma = 43/18$, $\tau = 187/91$ and $\sigma = 36/91$. We also show in the bottom three rows the calculation of η, δ and σ by using the scaling relations in Eqs. (12) and (13) which can be compared with the measured values of the exponents.

Applied stress (f)	0.10	0.12	0.14	0.16	0.18
d_c	0.543 ± 0.001	0.537 ± 0.001	0.522 ± 0.001	0.503 ± 0.001	0.485 ± 0.001
β	0.20 ± 0.05	0.19 ± 0.06	0.21 ± 0.04	0.23 ± 0.07	0.18 ± 0.05
γ	2.43 ± 0.03	2.40 ± 0.04	2.39 ± 0.03	2.45 ± 0.02	2.44 ± 0.02
δ	4.87 ± 0.05	4.83 ± 0.04	4.89 ± 0.03	4.88 ± 0.02	4.92 ± 0.02
η	7.20 ± 0.07	7.23 ± 0.09	7.15 ± 0.08	7.20 ± 0.09	7.19 ± 0.07
τ	2.06 ± 0.05	2.03 ± 0.04	2.07 ± 0.04	2.06 ± 0.02	2.10 ± 0.03
σ	0.40 ± 0.02	0.39 ± 0.04	0.43 ± 0.03	0.41 ± 0.02	0.38 ± 0.03
δ (Eq. (13))	5.06 ± 0.11	4.99 ± 0.14	4.99 ± 0.10	5.13 ± 0.11	5.06 ± 0.09
η (Eq. (13))	7.31 ± 0.13	7.26 ± 0.12	7.39 ± 0.09	7.31 ± 0.06	7.40 ± 0.06
σ (Eq. (12))	0.37 ± 0.12	0.34 ± 0.16	0.38 ± 0.12	0.36 ± 0.14	0.43 ± 0.15

Using Eq. (10), we have the scaling relations connecting the moment exponents with τ and σ,

$$\beta = (\tau - 2)/\sigma \quad , \qquad \gamma = (3 - \tau)/\sigma \quad , \qquad \delta = (4 - \tau)/\sigma \qquad \text{and} \qquad \eta = (5 - \tau)/\sigma \ . \tag{12}$$

Furthermore, we can eliminate τ and σ to find the scaling relations between the moment exponents,

$$\delta = \beta + 2\gamma \qquad \text{and} \qquad \eta = 2\delta - \gamma \ . \tag{13}$$

In Fig. 6, we plot the moments for $T = 0.06$ and $f = 0.10$. From the slopes, we find the values of the exponents, $\gamma = 2.43 \pm 0.03$, $\delta = 4.87 \pm 0.05$ and $\eta = 7.20 \pm 0.07$. The values are close to those of site percolation model in 2D. The exponents satisfy the relationship given in Eqs. (12) and (13) within error bar. The full list of exponents for different values of the applied stress f is listed in Table 1 where the verification of the scaling relations in Eqs. (12) and (13) are also indicated.

3.3. Boundary between the random and localized failure

We show in Fig. 7, the variation of the critical damage d_c with the applied stress f for $T = 0.06$. The system undergoes a percolation transition at d_c. The value of d_c decreases with the increase in f for $f < f_c$. Above f_c, there is a crossover in the failure process from a percolation type growth to a compact localized growth where the geometrical quantities show different behavior as observed in Fig. 3. To find the boundary between the random failure from the localized fracture growth as a function of temperature, we focus on the largest perimeter size $h_{\max}$ which shows abrupt decrease in the peak value when the applied stress crosses f_c. As mentioned before, this is due to the fractal structure of the percolation clusters at d_c which makes the hull highly rarefied and long compared to the perimeters of the compact clusters in the localized growth [50]. Two such clusters are shown in Fig. 8(a) and (b) for the percolation type growth and the localized growth respectively where the largest clusters are colored by white. In Fig. 8(c), we plot h_{peak}, the maximum value of the largest perimeter size $h_{\max}$ during a failure process, as a function of the applied stress f for three different temperatures $T = 0.06$, 0.08 and 0.10. The plots show two distinct regimes, regime (I) with fairly constant higher values and regime (II)

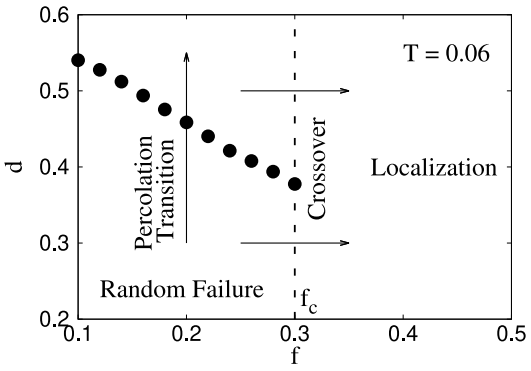

Fig. 7. The two different regimes in the d vs f plane: the (I) random failure and (II) localization, depending on whether the applied stress is below or above f_c, the crossover point. For $f > f_c$, compact clusters grow in the bundle. For $f < f_c$, the failure process is random and the model undergoes a percolation transition around the critical damage d_c indicated by the black dots. We kept $T = 0.06$ and $D = 0.02$ here.

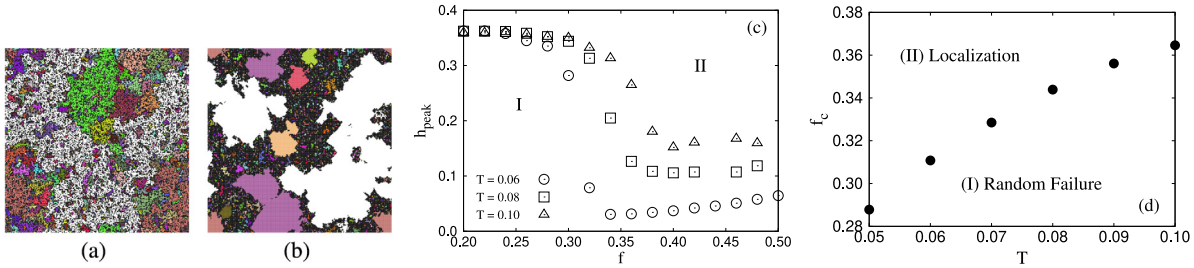

Fig. 8. Snapshots of the system for (a) non-localized ($f = 0.1$) and (b) localized ($f = 0.4$) growths when a spanning cluster appears in the system. The largest cluster is marked by white. In (c), we show the variation of h_{peak} with applied stress f where h_{peak} has a high value at low applied stress. As f is increased beyond a threshold value f_c, h_{peak} decreases rapidly and saturates at sufficiently low value. In (d) we show the boundary separating two different regimes, (I) the percolation type random failure and (II) the localized crack growth. As temperature increases, the localization takes place at a relatively higher applied stress as the stress concentration has to overcome a larger thermal randomness.

where h_{peak} falls rapidly to a relatively lower value as f crosses f_c. By measuring the values of f_c for different temperatures, we find the boundary on the f_c vs T plane that separates the random failure (I) from the localized failure (II). This is shown in Fig. 8 (d). As the temperature is increased, a higher applied stress is required to establish localization in the model. This is because the increase in temperature increases thermal fluctuations that lead to higher spatial randomness in the failure events. In this case, a large amount of stress localization is required to counteract the thermal fluctuation.

4. Conclusions

We have included thermal noise in an LLS fiber bundle model and studied creep failure through the interplay between thermal fluctuations and stress concentration due to externally applied stress. We observed that the presence of thermal fluctuations makes the failure events spatially uncorrelated and non-localized even if the strength of system disorder is low. This non-localized fracture growth shows a percolation type transition governed by critical exponents and scaling relations. For homogeneous fiber bundles without any system disorder, a complex phase space was explored for thermally activated failures in LLS with a different failure criteria [23]. There, in additions to a percolation type phase transition similar to the one observed here, an abrupt first-order phase transition was also observed depending on the stress and temperature. Two types of phase transitions have also been observed recently in LLS fiber bundle in the absence of temperature where the order of transition depends on how the system disorder is tuned [44]. There, a correlated fracture growth was observed in the low-disorder regime which is similar to invasion percolation. Such spatial correlation may also be obtained in the presence of temperature as well when the applied stress is sufficiently high so that the effect of stress localization can outrun the effect of thermal fluctuations. Stormo et al. [37] observed localized failure in a soft clamp model [36] when the elasticity of the clamps were decreased. In fiber bundle model the disorder strength and the stress release range play crucial role in determining the correlations in space. One can also approach a random failure process by increasing the stress release range instead of the disorder strength [51,52]. Our present study explores the effect of temperature on correlated fracture growth and shows that a larger stress has to be applied to overcome the thermal fluctuations and to initiate localization.

Finally, we point out here that the percolation transition during the non-localized fracture growth can also be observed for a bundle with uniform threshold distribution with a narrow width. We performed simulations with uniform threshold

distribution spanning from 0.6 to 0.9 and measured the critical exponents. The exponents we found are the same as those reported here within error bar. However, the crossover between the localized and non-localized regimes strongly depends on the disorder as we have seen previously in the case of no temperature [44]. In the presence of temperature, how a change in the system disorder will affect the crossover is therefore an open question.

Declaration of competing interest

The authors declare that they have no known competing financial interests or personal relationships that could have appeared to influence the work reported in this paper.

Acknowledgments

This work was partly supported by the Research Council of Norway through its Centers of Excellence funding scheme, project number 262644 and by the National Natural Science Foundation of China under grant number 11750110430.

References

[1] H.J. Herrmann, S. Roux (Eds.), Statistical Models for the Fracture of Disordered Media, Elsevier, Amsterdam, 2014.
[2] B.R. Lawn, Fracture of Brittle Solids, Cambridge University Press, Cambridge, 1993.
[3] T. Wong, P. Baud, The brittle–ductile transition in porous rock: A review, J. Struct. Geol. 44 (2012) 25.
[4] H. Charan, A. Hansen, H.G.E. Hentschel, I. Procaccia, Fatigue and failure of a polymer chain under tension, 2020, https://arxiv.org/abs/2008.00970.
[5] B. Voight, A relation to describe rate-dependent material failure, Science 243 (1989) 200.
[6] I.G. Main, A damage mechanics model for power-law creep and earthquake aftershock and foreshock sequences, Geophys. J. Int. 142 (2000) 151.
[7] H. Nechad, A. Helmstetter, R. El. Guerjouma, D. Sornette, Andrade and critical time-to-failure laws in fiber-matrix composites: Experiments and model, J. Mech. Phys. Solids 53 (2005) 1099.
[8] F.T. Peirce, Tensile tests for cotton yarns: Theorems on the strength of long and of composite specimens, J. Text. Ind. 17 (1926) 355.
[9] H.E. Daniels, The statistical theory of the strength of bundles of threads. I, Proc. R. Soc. London Ser. A 183 (1945) 405.
[10] H.J. Herrmann, S. Roux, Statistical Models for the Fracture of Disordered Media, North Holland, Amsterdam, 1990.
[11] B.K. Chakrabarti, L.G. Benguigui, Statistical Physics of Fracture and Breakdown in Disordered Systems, Oxford University Press, Oxford, 1997.
[12] S. Pradhan, A. Hansen, B.K. Chakrabarti, Failure processes in elastic fiber bundles, Rev. Modern Phys. 82 (2010) 499.
[13] A. Hansen, P.C. Hemmer, S. Pradhan, The Fiber Bundle Model: Modeling Failure in Materials, WILEY-VCH, 2015.
[14] S. Biswas, P. Ray, B.K. Chakrabarti, Statistical Physics of Fracture, Beakdown, and Earthquake: Effects of Disorder and Heterogeneity, WILEY-VCH, 2015.
[15] S. Ciliberto, A. Guarino, R. Scorretti, The effect of disorder on the fracture nucleation process, Physica D 158 (2001) 83.
[16] R. Scorretti, S. Ciliberto, A. Guarino, Disorder enhances the effects of thermal noise in the fiber bundle model, Europhys. Lett. 55 (2001) 626.
[17] A. Politi, S. Ciliberto, R. Scorretti, Failure time in the fiber-bundle model with thermal noise and disorder, Phys. Rev. E 66 (2002) 026107.
[18] A. Saichev, D. Sornette, Andrade, omori, and time-to-failure laws from thermal noise in material rupture, Phys. Rev. E 71 (2005) 016608.
[19] S. Pradhan, B.K. Chakrabarti, Failure due to fatigue in fiber bundles and solids, Phys. Rev. E 67 (2003) 046124.
[20] S. Pradhan, A.K. Chandra, B.K. Chakrabarti, Noise-induced rupture process: Phase boundary and scaling of waiting time distribution, Phys. Rev. E 88 (2013) 012123.
[21] Z. Danku, F. Kun, Creep rupture as a non-homogeneous Poissonian process, Sci. Rep. 3 (2013) 2688.
[22] N. Yoshioka, F. Kun, N. Ito, Size scaling and bursting activity in thermally activated breakdown of fiber bundles, Phys. Rev. Lett. 101 (2008) 145502.
[23] N. Yoshioka, F. Kun, N. Ito, Kertész line of thermally activated breakdown phenomena, Phys. Rev. E 82 (2010) 055102(R).
[24] R.C. Hidalgo, F. Kun, H.J. Herrmann, Creep rupture of viscoelastic fiber bundles, Phys. Rev. E 65 (2002) 032502.
[25] F. Kun, Y. Moreno, R.C. Hidalgo, H.J. Herrmann, Creep rupture has two universality classes, Europhys. Lett. 63 (2003) 347.
[26] S. Roy, S. Biswas, P. Ray, Failure time in heterogeneous systems, Phys. Rev. Res. 1 (2019) 033047.
[27] S. Roy, T. Hatano, Creeplike behavior in athermal threshold dynamics: Effects of disorder and stress, Phys. Rev. E 97 (2018) 062149.
[28] D. Sornette, Mean-field solution of a block-spring model of earthquakes, J. Phys. I France 2 (1992) 2089.
[29] P.C. Hemmer, A. Hansen, The distribution of simultaneous fiber failures in fiber bundles, J. Appl. Mech. 59 (1992) 909.
[30] A. Hansen, P.C. Hemmer, Burst avalanches in bundles of fibers: Local versus global load-sharing, Phys. Lett. A 184 (1994) 394.
[31] S.D. Zhang, E.J. Ding, Burst-size distribution in fiber-bundles with local load-sharing, Phys. Lett. A 193 (1994) 425.
[32] M. Kloster, A. Hansen, P.C. Hemmer, Burst avalanches in solvable models of fibrous materials, Phys. Rev. E 56 (1997) 2615.
[33] D.G. Harlow, S.L. Phoenix, The chain-of-bundles probability model for the strength of fibrous materials II: A numerical study of convergence, J. Compos. Mater. 12 (1978) 314.
[34] D.G. Harlow, S.L. Phoenix, Approximations for the strength distribution and size effect in an idealized lattice model of material breakdown, J. Mech. Phys. Solids 39 (1991) 173.
[35] R.C. Hidalgo, Y. Moreno, F. Kun, H.J. Herrmann, Fracture model with variable range of interaction, Phys. Rev. E 65 (2002) 046148.
[36] G.G. Batrouni, A. Hansen, J. Schmittbuhl, Heterogeneous interfacial failure between two elastic blocks, Phys. Rev. E 65 (2002) 036126.
[37] A. Stormo, K.S. Gjerden, A. Hansen, Onset of localization in heterogeneous interfacial failure, Phys. Rev. E 86 (2012) 025101(R).
[38] K.S. Gjerden, A. Stormo, A. Hansen, Universality classes in constrained crack growth, Phys. Rev. Lett. 111 (2013) 135502.
[39] K.S. Gjerden, A. Stormo, A. Hansen, Local dynamics of a randomly pinned crack front: A numerical study, Front. Phys. 2 (2014) 66.
[40] S. Sinha, J.T. Kjellstadli, A. Hansen, Local load-sharing fiber bundle model in higher dimensions, Phys. Rev. E 92 (2015) 020401.
[41] D. Stauffer, Scaling theory of percolation clusters, Phys. Rep. 54 (1979) 1.
[42] D. Stauffer, A. Aharony, Introduction to Percolation Theory, second ed., Taylor and Francis, London, 1995.
[43] T. Grossman, A. Aharony, Accessible external perimeters of percolation clusters, J. Phys. A: Math. Gen. 20 (1987) L1193.
[44] S. Sinha, S. Roy, A. Hansen, Phase transitions and correlations in fracture processes where disorder and stress compete, Phys. Rev. Res. 2 (2020) 043108.
[45] S. Roy, T. Hatano, Creep failure in a threshold-activated dynamics: Role of temperature during a subcritical loading, Phys. Rev. Res. 2 (2020) 023104.
[46] A. Hansen, E.L. Hinrichsen, S. Roux, Scale-invariant disorder in fracture and related breakdown phenomena, Phys. Rev. B 43 (1991) 665.

[47] B. Skjetne, A. Hansen, Implications of realistic fracture criteria on crack morphology, Front. Phys. 7 (2019) 50.
[48] S.B. Santra, Directed spiral site percolation on the square lattice, Eur. Phys. J. B 33 (2003) 75.
[49] S. Sinha, S.B. Santra, Breakdown of universality in directed spiral percolation, Eur. Phys. J. B 39 (2004) 513.
[50] S. Sinha, S.B. Santra, Directed spiral percolation hull on the square and triangular lattice, Internat. J. Modern Phys. C 16 (2005) 1251.
[51] S. Biswas, S. Roy, P. Ray, Nucleation versus percolation: Scaling criterion for failure in disordered solids, Phys. Rev. E 91 (2015) 050105(R).
[52] S. Roy, S. Biswas, P. Ray, Modes of failure in disordered solids, Phys. Rev. E 96 (2017) 063003.